

# Redshift Evolution of Galaxy Cluster Densities

R. G. Carlberg<sup>1,2</sup>, S. L. Morris<sup>1,3</sup>, H. K. C. Yee<sup>1,2</sup>, & E. Ellingson<sup>1,4</sup>,

## ABSTRACT

The number of rich galaxy clusters per unit volume is a strong function of  $\Omega$ , the cosmological density parameter, and  $\sigma_8$ , the linear extrapolation to  $z = 0$  of the density contrast in  $8h^{-1}$  Mpc spheres. The CNOC cluster redshift survey provides a sample of clusters whose average mass profiles are accurately known, which enables a secure association between cluster numbers and the filtered density perturbation spectrum. We select from the CNOC cluster survey those EMSS clusters with bolometric  $L_x \geq 10^{45}$  erg s $^{-1}$  and a velocity dispersion exceeding 800 km s $^{-1}$  in the redshift ranges 0.18-0.35 and 0.35-0.55. We compare the number density of these subsamples with similar samples at both high and low redshift. Using the Press-Schechter formalism and CDM style structure models, the density data are best described with  $\sigma_8 \simeq 0.75 \pm 0.1$  and  $\Omega \simeq 0.4 \pm 0.2$  (90% confidence). The cluster dynamical analysis gives  $\Omega = 0.2 \pm 0.1$  for which  $\sigma_8 = 0.95 \pm 0.1$  (90% confidence). The predicted cluster density evolution in an  $\Omega = 1$  CDM model exceeds that observed by more than an order of magnitude.

*Subject headings:* galaxies: clusters, cosmology: large-scale structure of universe

## 1. Introduction

The clustering of galaxies grows via gravity from density perturbations which are characterized by their power spectrum,  $P(k)$ . Various theories predict the shape of  $P(k)$ , but they do not accurately predict its amplitude. An integral constraint on the normalization is conventionally parameterized as  $\sigma_8$ , the fractional mass variance in  $8 h^{-1}$  Mpc spheres calculated using the linear extrapolation of  $P(k)$ . Rich galaxy clusters are particularly sensitive probes of  $\sigma_8$ . N-body simulations have established that the Press-Schechter formalism (Press & Schechter 1974, hereafter PS) gives a remarkably accurate prediction of the number of clusters per unit cosmological volume

---

<sup>1</sup>Visiting Astronomer, Canada-France-Hawaii Telescope, which is operated by the National Research Council of Canada, le Centre National de Recherche Scientifique, and the University of Hawaii.

<sup>2</sup>Department of Astronomy, University of Toronto, Toronto ON, M5S 3H8 Canada

<sup>3</sup>Dominion Astrophysical Observatory, Herzberg Institute of Astrophysics, National Research Council of Canada, 5071 West Saanich Road, Victoria, BC, V8X 4M6, Canada

<sup>4</sup>Center for Astrophysics & Space Astronomy, University of Colorado, CO 80309, USA

as a function of mass. Modeling the low redshift data with the Press-Schechter formula, and using CDM style  $P(k)$ , leads to a range of possibilities, from  $\Omega = 1$  and  $\sigma_8 \simeq 0.5$  to  $\Omega \simeq 0.2$  and  $\sigma_8 \simeq 1$  and values that interpolate between the two (Henry & Arnaud 1991, White, Efstathiou & Frenk 1993, Eke, Cole & Frenk 1996, Viana & Liddle 1996, Bond & Myers 1996). The  $\Omega$  dependence can be disentangled from  $\sigma_8$  if data giving  $n(M) dM$  are available as a function of redshift (Oukbir & Blanchard 1996).

The Canadian Network for Observational Cosmology (CNOC) cluster sample and observational strategy (Yee, Ellingson & Carlberg 1996) was specifically designed to produce data useful for a  $\sigma_8$  measurement. The sample’s primary advantage is that the cluster masses are accurately known near the virial radius which is essential for a reliable estimate of the linear mass scale from which the cluster collapsed. Here we combine our results with similarly selected clusters at higher and lower redshifts in Section 3. The data are modeled in Section 4 to draw conclusions about the values of  $\sigma_8$  and  $\Omega$ .

## 2. Press-Schechter Predictions

The number density of clusters in the mass range  $M$  to  $M + dM$  is predicted to be

$$n(M) dM = \frac{-3\delta_c(z)}{(2\pi r_L^2)^{3/2} \Delta} \frac{d \ln \Delta}{d M} \exp[-\delta_c^2(z)/2\Delta^2] dM, \quad (1)$$

where  $\delta_c(z) = \delta_0(\Omega)/D(z, \Omega)$  gives the linear overdensity at which a collapsed structure is approximately virialized. The function  $\delta_0 = 0.15(12\pi)^{2/3}\Omega^{0.0185}$  is nearly constant at  $\delta_0 \simeq 1.68$  (Navarro, Frenk & White 1996). The growth factor,  $D(z, \Omega)$ , gives the redshift dependence of the linear amplitude of the density perturbations (Peebles 1993). The quantity  $\Delta(r_L)$  measures the fractional linear mass variance in spheres of radius  $r_L$ . It is calculated using a tophat filter from a parameterized version of the CDM spectrum ( $\Gamma$  fixed at 0.2 Efstathiou, Bond & White 1992) whose normalization is adjusted such that  $\sigma_8 = \Delta(8h^{-1}\text{Mpc})$ . The “just virialized” radius is near  $1.5h^{-1}\text{Mpc}$  and has an overdensity of  $\simeq 178\Omega^{-0.6}$  (White, Efstathiou & Frenk 1993). Near  $1.5h^{-1}\text{Mpc}$   $M(r) \propto r^p$ , where  $p \simeq 0.64$  for the CNOC data (Carlberg, Yee & Ellingson 1997). The tophat filtering scale,  $r_L$ , is related to  $M_{1.5}$ , as  $r_L \simeq 8.43\Omega(z)^{0.2p/(3-p)} [M_{1.5}/6.97 \times 10^{14}h^{-1}\text{M}_\odot/\Omega]^{1/(3-p)} (1+z)^{-p/(3-p)} h^{-1}\text{Mpc}$  (a generalization of White, Efstathiou & Frenk 1993) where  $\Omega(z)$  is the value of  $\Omega$  at redshift  $z$ .

We integrate Eq. 1 from the minimum mass in the sample to infinity to derive  $n(> M_{1.5})$ . For comparison with measurements, we average the density predictions over the redshift ranges of interest. These predictions are plotted in Figures 1 and 2 for  $\Omega = 0.2$  and  $\Omega = 1$ , respectively.

### 3. Cluster Density Estimates

The CNOC sample was drawn from the EMSS cluster survey (Henry *et al.* 1992), supplemented with a few high redshift clusters identified later (Luppino & Gioia 1995). We impose the constraints  $f_x \geq 4 \times 10^{-13} \text{ erg cm}^{-2} \text{ s}^{-1}$ ,  $L_x(0.3 - 3.5 \text{ Kev}) \geq 4 \times 10^{44} \text{ erg s}^{-1}$ , redshifts between 0.18 and 0.55, and in the declination range  $-15$  to  $+65$  degrees. We have recalculated the  $f_x$  and  $L_x$  to better allow for the redshift dependence of the flux in the “detect cell”. The main difference is that the cluster MS0302+16 now falls below our luminosity cut, although this has a negligible affect on the results (see also Nichol, *et al.* 1997).

The  $M_{1.5}$  masses for each cluster in the CNOC sample are estimated to be  $M_v b_{Mv} (1.5h^{-1} \text{ Mpc}/r_v)^p$  where  $b_{Mv}$  is the virial mass bias,  $r_v$  is the virial radius, calculated as a ringwise potential (Carlberg *et al.* 1996), and  $M_v$  is the resulting virial mass. For the CNOC clusters  $b_{Mv} \simeq 0.85$  on the average (Carlberg, Yee & Ellingson 1997), that is, the virial mass is always an overestimate. The masses  $M_{1.5}$  are calculated from the  $M_v$  and  $r_v$  of the CNOC clusters (Carlberg *et al.* 1996 as updated slightly by the use of the finalized catalogues).

#### 3.1. Correcting for X-Ray Selection

We need to count the number of clusters having  $M_{1.5}$  larger than a specified mass within some redshift range. A significant complication is that we have a sample defined by its X-ray properties, but we want to make a measurement based on its distribution of characteristic masses. It is well known that there is a strong  $L_x - M_{1.5}$  correlation, but with a substantial scatter (for instance, Edge & Stewart 1991, hereafter ES). That is, some clusters that are in the  $L_x$  limited sample will be below the specified mass limit and vice versa. To correct from an X-ray selected sample to a mass selected sample we proceed as follows. We use the Edge and Stewart study of the X-ray and optical properties of nearby clusters, which appear to be essentially identical to the CNOC sample in the relevant parameters, see Figure 3. The ES sample is effectively a mass selected sample, at least for the rich clusters which are our concern here. All the selected clusters have a bolometric  $L_x \geq 10^{45} \text{ erg s}^{-1}$ . Examining Figure 3, we see that setting the minimum mass equal to that for a cluster with  $\sigma_v \simeq 800 \text{ km s}^{-1}$  will help maximize the number of clusters in the sample while keeping the corrections from the  $L_x$  selected sample to the  $\sigma_v$  selected sample relatively small.

There are two different correction factors for  $L_x$  defined samples, depending on whether or not the parent sample has known velocity dispersions. In the ES sample there are 12 clusters with  $\sigma_v \geq 800 \text{ km s}^{-1}$ , of which 6 are also above  $L_x \geq 10^{45} \text{ erg s}^{-1}$ . Therefore we estimate that for a sample selected with both the  $L_x$  and  $\sigma_v$  limits, the true density of clusters with  $\sigma_v \geq 800 \text{ km s}^{-1}$  is a factor of  $f_{x\sigma} = 12/6 = 2 \pm 1$  times the density measured. There are 8 ES clusters with  $L_x \geq 10^{45} \text{ erg s}^{-1}$  for all velocity dispersions and 12 with  $\sigma_v \geq 800 \text{ km s}^{-1}$ . Therefore for a sample selected with only the  $L_x$  limit, we estimate that the number of clusters above  $\sigma_v = 800 \text{ km s}^{-1}$  is  $f_x = 12/8 = 1.5 \pm 0.7$  times the measured density. Although these corrections are not very

accurate, they illustrate that the corrections are not large, and their errors are comparable in size to those from the subsamples themselves.

### 3.2. The CNOC Sample

To convert from EMSS 0.3-3.5Kev luminosities to the bolometric luminosity we derive a mean bolometric correction of a factor of 2.20 at 6.8 Kev and 3.12 at 13.6 Kev, with only a small dependence on the HI column. We adopt a uniform bolometric correction of a factor of 2.5 for the CNOC clusters (see the high  $L_x$  sample of Henry, Jiao & Gioia 1994 for representative EMSS cluster temperatures). Imposing the limit  $\sigma_v \geq 800 \text{ km s}^{-1}$  reduces the CNOC sample size from 12 clusters to 8 (2 of the 16 clusters observed being dropped as being below the X-ray limits, 1 cluster not from EMSS, and 1 has a poorly determined  $\sigma_v$ ). Using the  $V_e/V_{max}$  method (Avni & Bahcall 1980) we then measure the volume density of these clusters, allowing for the EMSS sky area in the CNOC region as a function of flux (see Henry *et al.* 1992 for more details on this procedure and also an example table of EMSS all-sky coverage). The mean densities of these clusters for  $\Omega = 0.2$  are reported in Table 1. The CNOC sample is split into a low redshift subsample,  $0.18 \leq z \leq 0.35$ , which has a smallest  $M_{1.5}$  of  $4.8 \times 10^{14} h^{-1} \text{ M}_\odot$  and a moderate redshift subsample,  $0.35 \leq z \leq 0.55$ , which is found to have a smallest  $M_{1.5}$  of  $6.7 \times 10^{14} h^{-1} \text{ M}_\odot$ . The  $f_{x\sigma}$  corrected densities are given in Table 1.

### 3.3. Low-Redshift Samples

At low redshift there are several samples to consider as sources of density estimates. The most straightforward dataset is that of Henry & Arnaud (1991, hereafter HA) who provide an X-ray luminosity function at low redshift, which when integrated from  $L_x = 10^{45} \text{ erg s}^{-1}$  to infinity yields an ( $f_x$  corrected) volume density of  $\simeq 7.5 \times 10^{-7} h^3 \text{ Mpc}^{-3}$ . The velocity dispersions of these clusters extend below  $800 \text{ km s}^{-1}$ , but none below  $750 \text{ km s}^{-1}$  (Zabludoff, Huchra, & Geller 1990), which we adopt as the minimum velocity dispersion. We scale the cluster masses with velocity dispersion as  $M \propto \sigma_v^3$  with a reference value of  $5.7 \times 10^{14} h^{-1} \text{ M}_\odot$ . We estimate the  $M_{1.5}$  of the HA sample as  $4.7 \times 10^{14} h^{-1} \text{ M}_\odot$ .

The ESO Cluster Survey (Mazure *et al.* 1996) finds a cluster density of  $2.5 \times 10^{-6} h^3 \text{ Mpc}^{-3}$  for  $\sigma_v \geq 800 \text{ km s}^{-1}$  at  $z \leq 0.1$ . However, the ESO and CNOC velocity dispersions are not calculated in the same manner. The CNOC velocity dispersions are estimated using an explicit background subtraction. On the average we find that our velocity dispersions are about 7% lower than those calculated from precisely the same velocities using the iterated bi-weight estimator (Beers, Flynn & Gebhardt 1990, Carlberg, Yee & Ellingson 1997). As we increase the redshift range of the data given to the bi-weight estimator up to 25%, the velocity dispersion rises an average of 13% and then remains reasonably stable. We adjust the ESO velocity dispersions

downwards by 13%, to arrive a velocity dispersion of  $708 \text{ km s}^{-1}$ . We derive a mass limit for the  $\text{ESO} \geq 800 \text{ km s}^{-1}$  sample of  $M_{1.5} = 4.0 \times 10^{14} h^{-1} M_{\odot}$ . The sample is not X-ray selected so needs no density correction.

An upper limit to the low redshift density for the Northern Abell sample with velocity dispersions has been derived previously (White, Efstathiou & Frenk 1993). The same sample, when compared with X-ray results confirms that the median velocity dispersion is somewhat overestimated (Eke, Cole & Frenk 1996 referred to as ECF), and argues that the velocity dispersion is about  $650 \text{ km s}^{-1}$ . Because this sample is very similar to the ESO sample, we adopt the same minimum velocity dispersion as we derived above,  $708 \text{ km s}^{-1}$ , and hence the same minimum mass. This sample requires no density correction.

### 3.4. A High-Redshift Sample

The EMSS sample contains a fair sample of clusters ranging from redshifts of about 0.14 to redshift 0.83 (Henry *et al.* 1992, Luppino & Gioia 1995). The high redshift sample (Luppino & Gioia 1995) is cautiously assigned the same minimum mass,  $M_{1.5} = 4.7 \times 10^{14} h^{-1} M_{\odot}$  as we used for the HA subsample. Given the richness of these clusters we expect that the clusters actually have higher masses, consequently this is a conservative assumption. The mean density derived from the 4 clusters in the redshift range  $0.55 \leq z \leq 0.85$  for  $\Omega = 0.2$  and 1 is given in the Table and includes the  $f_x$  correction. Reassuringly, they are similar to the densities derived elsewhere (Luppino & Gioia 1995) using the same clusters, but a different analysis. It is known that at least one of these clusters, MS1054–03, likely has a mass well over the limit to be included in the sample (Luppino & Kaiser 1996). The minimum mass is uncertain but likely at least that of the moderate  $z$  CNOc sample. In particular, these are very rich clusters which the very strong richness- $\sigma_v$  relation (Carlberg *et al.* 1996) indicates to be high  $\sigma_v$  clusters. We expect  $\sigma_v \simeq 900 \text{ km s}^{-1}$ .

## 4. Parameter Probabilities and Conclusions

The  $\chi^2$  probability contours of the PS predictions and the observed densities are plotted in Figure 4. The sample variances are calculated as the quadrature sum of the  $1/\sqrt{N}$  of the sample and the errors in the sample correction factors. The observed densities as a function of  $\Omega$  are estimated as a linear interpolation between the values at  $\Omega = 0.2$  and  $\Omega = 1$  measurements. The mass errors are known to be about 25% for a single cluster (Carlberg *et al.* 1996), which in the mean for the various samples will be reduced to about 8-15%, depending on sample size. This relatively small error is neglected in calculating  $\chi^2$ .

The minimum  $\chi^2$  is near  $\Omega \simeq 0.4$  and  $\sigma_8 \simeq 0.75$ , although  $\Omega$  between 0.2 and 0.6 are statistically acceptable within the 90% confidence interval. For our preferred  $\Omega = 0.2$  we find that  $\sigma_8 = 0.95 \pm 0.05$ . A model with  $\Omega = 1$  is excluded at more than 99% confidence, although this is

dependent on the the estimated masses of the high redshift EMSS sample.

We thank Mike Hudson, Jim Bartlett, Alain Blanchard and Jamila Oukbir for comments. The Canadian Time Assignment Committee allocated CFHT observing time. The CFHT organization provided the technical support which made these observations feasible. Funding was provided by NSERC and NRC of Canada.

## REFERENCES

Avni, Y. & Bahcall, J. N. 1980, *ApJ*, 235, 694

Beers, T. C., Flynn, K., & Gebhardt, K. 1990, *AJ*, 100, 32

Bond, J. R. & Myers, S. T. 1996, *ApJS*, 103, 63

Carlberg, R. G., Yee, H. K. C., Ellingson, E., Abraham, R., Gravel, P., Morris, S. M., & Pritchett, C. J. 1996, *ApJ*, 462, 32

Carlberg, R. G., Yee, H. K. C., & Ellingson, E. 1997, *ApJ*, in press

Davis, M. & Peebles, P. J. E. 1983, *ApJ*, 267, 465

Edge, A. C. & Stewart, G. C. 1991, *MNRAS*, 252, 428

Efstathiou, G., Bond, J. R. & White, S. D. M. 1992, *MNRAS*, 258, 1P

Eke, V. R., Cole, S., & Frenk, C. S. 1996, *astro-ph/9601088*

Henry, J. P. & Arnaud, K. A. 1991, *ApJ*, 372, 410

Henry, J. P., Gioia, I. M., Maccacaro, T., Morris, S. L., Stocke, J. T., & Wolter, A. 1992, *ApJ*, 386, 408

Henry, J. P., Jiao, L., & Gioia, I. M. 1994, *ApJ*, 432, 49

Loveday, J., Maddox, S. J., Efstathiou, G., & Peterson, B. A. 1995, *ApJ*, 442, 457

Luppino, G. A. & Gioia, I. M. 1995, *ApJ*, 445, 77L

Luppino, G. A. & Kaiser, N. 1996, *astro-ph/9601094*

Mazure, A., Katgert, P., den Hartog, R., Biviano, A., Dubath, P., Escalara, E., Focardi, P., Gerbal, D., Giuricin, G., Jones, B., Le Fèvre, O., Moles, M., Perea, J., & Rhee, G. 1996, *A&A*, 310, 31

Navarro, J. F., Frenk, C. S., & White, S. D. M. 1996, *ApJ*, submitted (*astro-ph/9611107*)

Nichol, R. C., Holden, B. P., Romer, A. K., Ulmer, M. P., Burke, D. J., & Collins, C. A. 1997, ApJ, submitted (astro-ph/9611182)

Oukbir, J. & Blanchard, A. 1996, A&A, submitted (also astro-ph/9611085)

Peebles, P. J. E. 1993, *Principles of Physical Cosmology* (Princeton University Press: Princeton)

Press, W. H. & Schechter, P. 1974, ApJ, 187, 425

Tucker, D.L., Oemler, A. Jr., Kirshner, R.P., Lin H., Shectman, S.A., Landy, S.D., Schechter, P.L., Müller, V., Gottlöber, S., and Einasto, J. 1996, MNRAS, submitted.

Viana, P. T. P. & Liddle, A. R. 1996, MNRAS, 281, 323

White, S. D. M., Efstathiou, G., & Frenk, C. S. 1993, MNRAS, 262, 1023

Yee, H. K. C., Ellingson, E., & Carlberg, R. G. 1996, ApJS, 102, 269

Zabludoff, A. I., Huchra, J. P., & Geller, M. J. 1990, ApJS, 74, 1

Table 1: Cluster Densities for  $\Omega = 0.2$ 

redshift	Sample	$\sigma_v$ (min)	$\log M$	$\log n(> M)$
		$\text{km s}^{-1}$	$h^{-1} \text{M}_\odot$	$\text{h}^{-3} \text{Mpc}^3$
0.0-0.10	WEF	850	14.66	-5.40
0.0-0.10	ECF	708	14.60	-5.40
0.0-0.10	ESO	708	14.60	-5.60
0.0-0.10	HA	750	14.67	-6.12
0.18-0.35	CNOC	800	14.68	-6.53
0.35-0.55	CNOC	800	14.80	-7.15
0.55-0.85	EMSS	800	14.81	-7.30

Fig. 1.— The  $n(> M)$  relation for the different redshift ranges as calculated from the PS formula for  $\Omega = 0.2$  and  $\sigma_8 = 0.95$ . The errors are  $N^{-1/2}$  estimates with the selection bias errors added in quadrature. Optically selected clusters have open symbols, X-ray selected clusters have closed symbols. The CNOC and EMSS samples have densities derived in this paper. The low redshift samples are discussed in the text.

Fig. 2.— The  $n(> M)$  relation from the PS formula calculated for  $\Omega = 1$  and  $\sigma_8 = 0.55$ . These model parameters do not adequately describe the data.

Fig. 3.— The bolometric X-ray luminosity versus line-of-sight velocity dispersion for the Edge & Stewart and CNOC samples. The sample limits at  $L_x \geq 10^{45} \text{ erg s}^{-1}$  and  $\sigma_v \geq 800 \text{ km s}^{-1}$  are shown. The ES velocity dispersions are divided by 1.13.

Fig. 4.— A plot of  $\chi^2$  for the all *independent* samples (solid lines) and excluding the high redshift EMSS sample (dotted lines). The contours are the 90% and 99% confidence levels. The results of the CNOC analysis,  $\Omega = 0.19 \pm 0.06$ , with its  $1\sigma$  range are indicated.

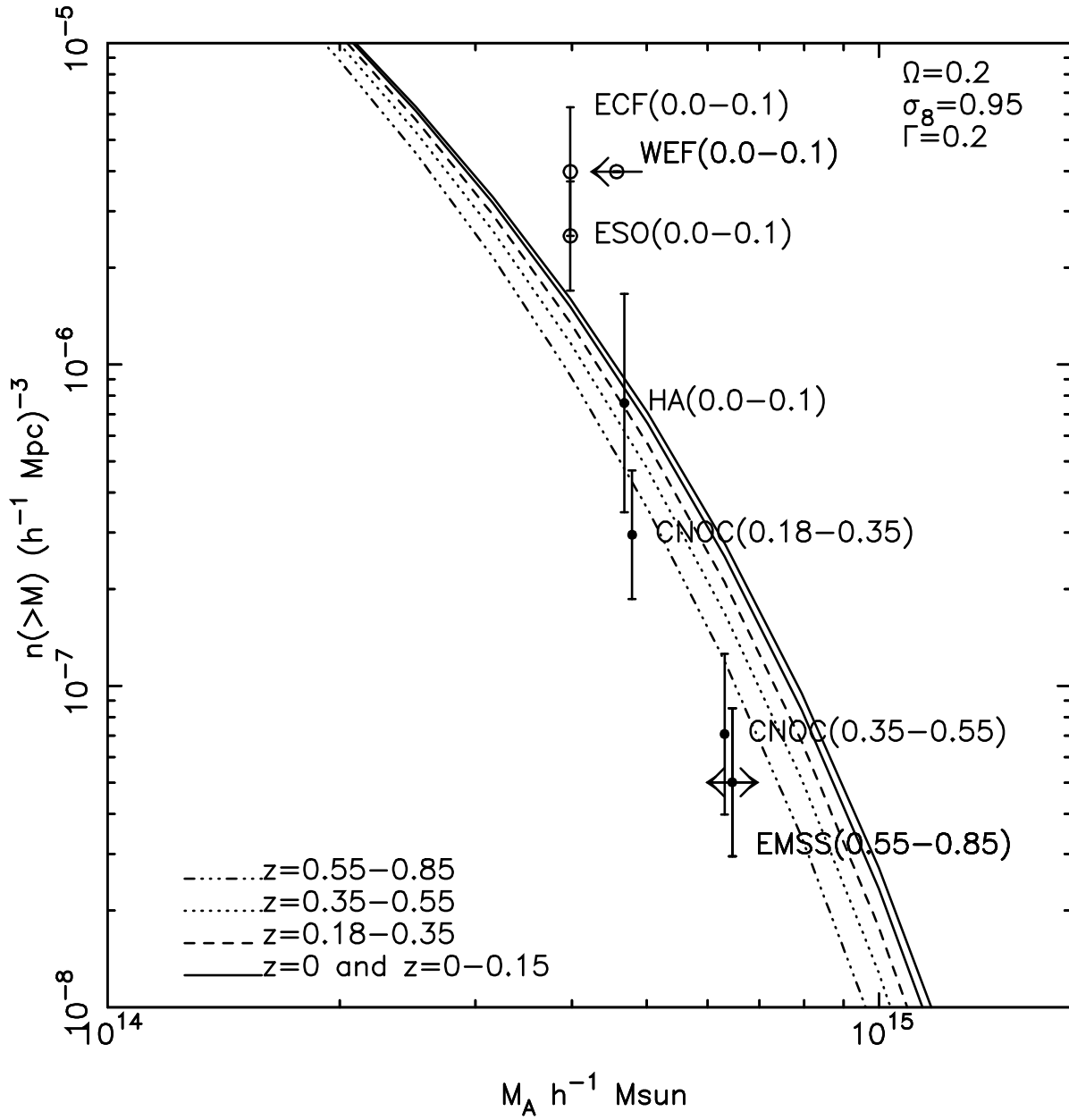


Fig. 1.— The  $n(>M)$  relation for the different redshift ranges as calculated from the PS formula for  $\Omega = 0.2$  and  $\sigma_8 = 0.95$ . The errors are  $N^{-1/2}$  estimates with the selection bias errors added in quadrature. Optically selected clusters have open symbols, X-ray selected clusters have closed symbols. The CNOC and EMSS samples have densities derived in this paper. The low redshift samples are discussed in the text.

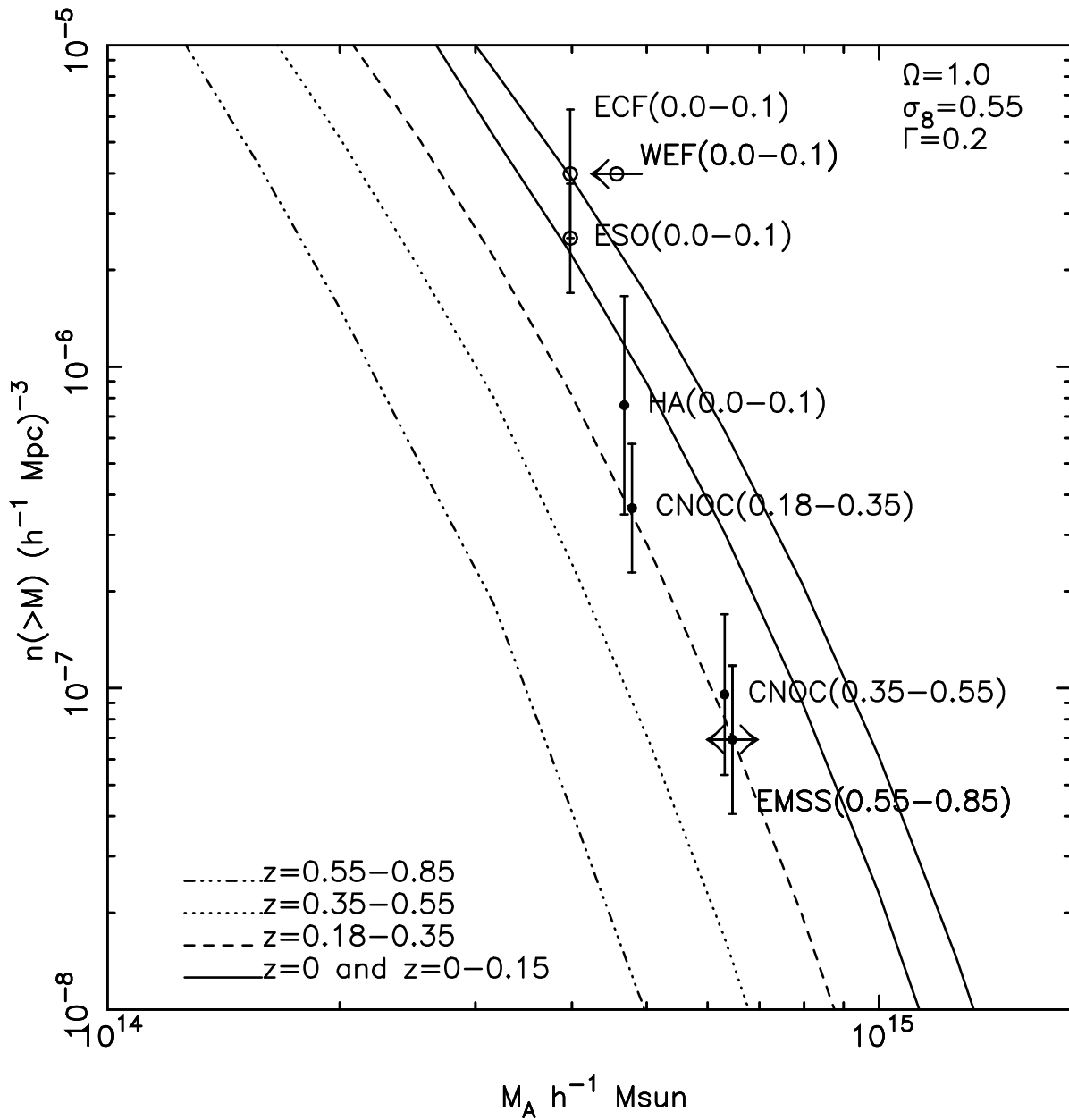


Fig. 2.— The  $n(> M)$  relation from the PS formula calculated for  $\Omega = 1$  and  $\sigma_8 = 0.55$ . These model parameters do not adequately describe the data.

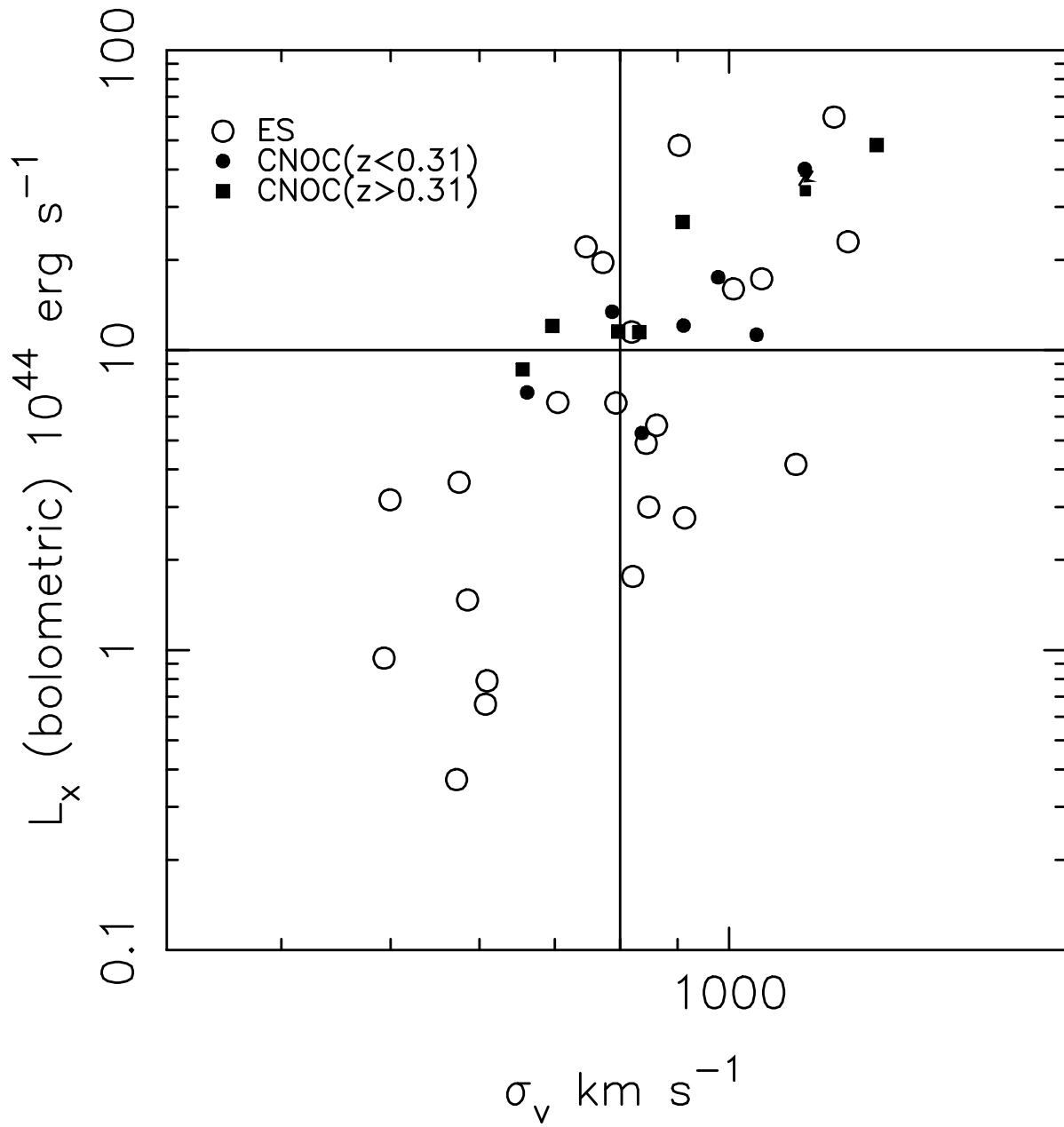


Fig. 3.— The bolometric X-ray luminosity versus line-of-sight velocity dispersion for the Edge & Stewart and CNOC samples. The sample limits at  $L_x \geq 10^{45} \text{ erg s}^{-1}$  and  $\sigma_v \geq 800 \text{ km s}^{-1}$  are shown. The ES velocity dispersions are divided by 1.13.

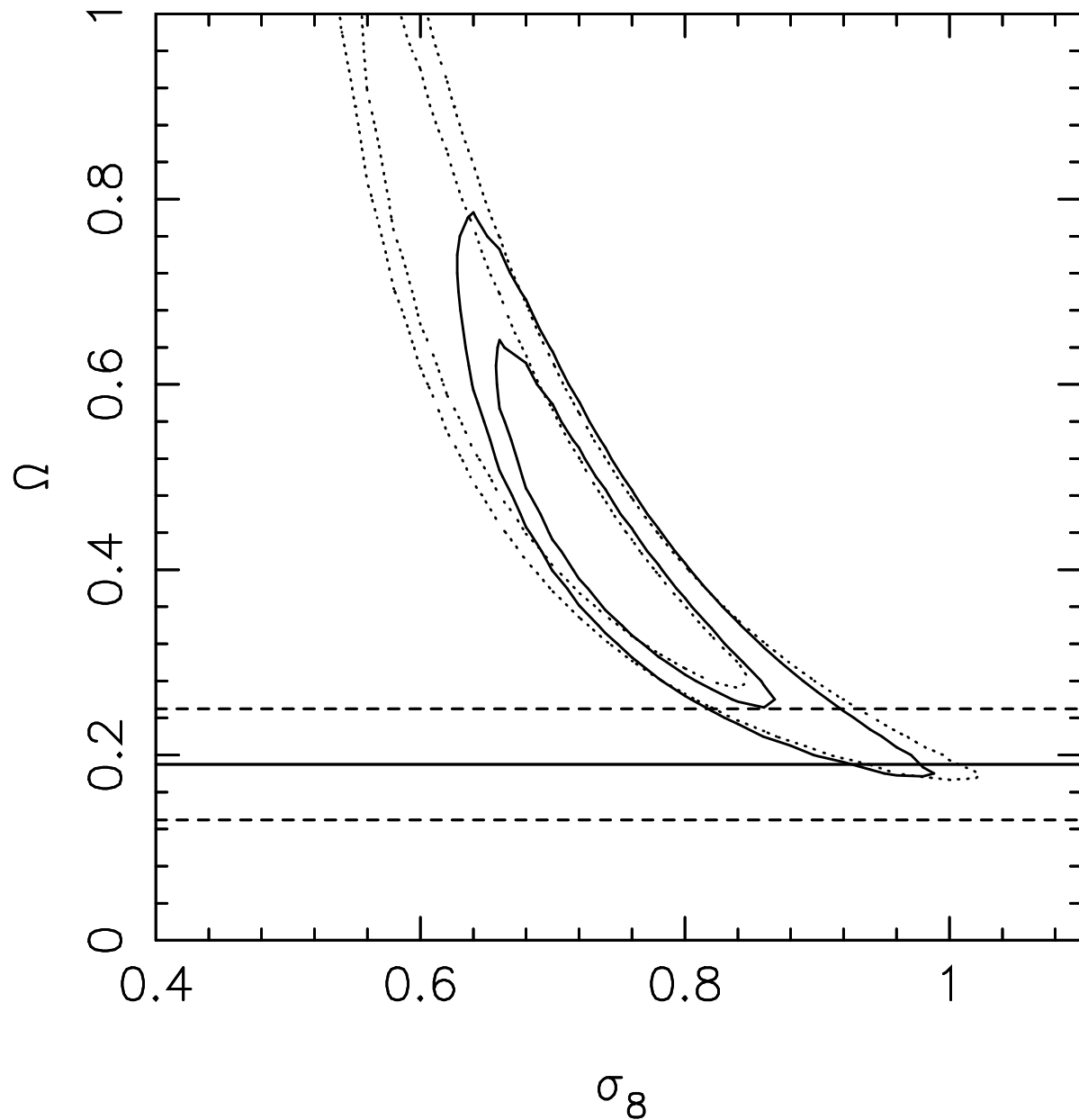


Fig. 4.— A plot of  $\chi^2$  for the all *independent* samples (solid lines) and excluding the high redshift EMSS sample (dotted lines). The contours are the 90% and 99% confidence levels. The results of the CNOC analysis,  $\Omega = 0.19 \pm 0.06$ , with its  $1\sigma$  range are indicated.